IOP Conf. Series: Materials Science and Engineering **371** (2018) 012035 doi:10.1088/1757-899X/371/1/012035

Seismic Performance of Steel Tube-high Strength Concrete Squat Walls

Z Z Zhao[1,2] , G Z Fan[1] , X G He[3] and X Liu[1]

1 Key Laboratory of Civil Engineering Safety and Durability of the China Education Ministry, Tsinghua University, Beijing 100084, China
2 Beijing Engineering Research Center of Steel and Concrete Composite Structures, Tsinghua University, Beijing 100084, China
3 Architectural Design and Research Institute of Tsinghua University, Tsinghua University, Beijing 100084, China
E-mail: fgz14@mails.tsinghua.edu.cn

Abstract. In order to investigate the seismic behaviour of the high strength concrete squat wall with distributed steel tubes, Three squat walls with steel tubes and one RC squat wall were tested. The strength, shear deformation, and energy dissipation capacity of these specimens were analyzed. The test results showed that the load-carrying capacity of the high strength concrete squat wall can be decreased after inserting steel tubes. However, the deformation capacity and the energy dissipation capacity of the squat wall can be improved dramatically when steel tubes are inserted into the section of the wall, especially the squat wall with steel tubes evenly distributed in the section, and as a result, it can be concluded that they are very suitable for application in the conversion layer to improve the collapse resistant capability of structures.

1. Introduction

Squat shear wall refers to the wall which the aspect ratio is less than 1.5. This type of wall is considered to exhibit poor ductile behavior due to the premature shear failure. Squat walls have been widely used in practical engineering, especially in walls that directly connected with foundation, that located on the upper part of the conversion layer, and that used in the nuclear engineering buildings [1, 2]. Because of the requirement for practical applications, many research works were carried out on the following related squat walls. Su et al. [3, 4] summarized and discussed the experimental data of four shaking table tests and numerical findings, and found that the phenomenon of shear concentration appeared at exterior walls above the transfer floor due to the local flexural deformation of transfer structures. The effect of shear concentration made the squat shear walls more prone to the occurrence of brittle failures, leading to the interrupt of the vertical load path and then the local collapse.

Based on the investigation of earthquake disaster and related researches [5-7], a new type squat shear wall with steel tubes distributed in the section was proposed in this study. This type of squat wall is supposed to enhance the deformation capacity and collapse resistant capability of structures making use of the advantages of concrete-filled steel tubes (CFSTs). In this paper, four high strength concrete squat shear walls with distributed steel tubes are designed and tested to investigate the seismic performance of this type wall. The shaped steel ratio and the arrangement of steel tubes are taken as major parameters. Based on the test data, an analysis of the failure modes, strength, stiffness degradation, ductility, and energy dissipation capacity of those specimens was conducted. The work in

this paper also provides a foundation for further development of a theoretical analysis, which will be discussed in another paper.

2. Experimental program

2.1. Test specimens

Four squat walls (SW1-SW4) with the same dimension were tested under cyclic loading. All the specimens had a height of 1080mm and a thickness of 160mm. The aspect ratio of the specimens was 0.95. The overall geometries of the squat walls are shown in Figure 1. The axial compression ratio of the specimens was the same, which was 0.35. Figure 2 shows the detailed sectional configurations of the specimens. SW1 was a RC squat wall taken as a comparative specimen. SW2 and SW3 were the squat walls with steel tubes arranged at both sides and the middle section of walls, respectively. SW4 was a squat wall with steel tubes evenly distributed in the cross-section of the specimen.

The outer diameter of the steel tube was 89mm, which was selected to match the size of specimens. The thickness of steel tubes was 4mm to ensure that the steel tube had sufficient constraint on the concrete filled in it. The diameter-to-thickness ratio of the steel tubes was 22.3. Steel tubes and vertical rebars were inserted into the foundation beam and top beam to ensure sufficient anchorage. The anchoring lengths of the vertical rebars and steel tubes were 650mm and 480mm, respectively. Four annular bars were welded at the bottom of each steel tube to anchor the steel tube into the foundation for the purpose of transferring the loads, as shown in Figure 1.

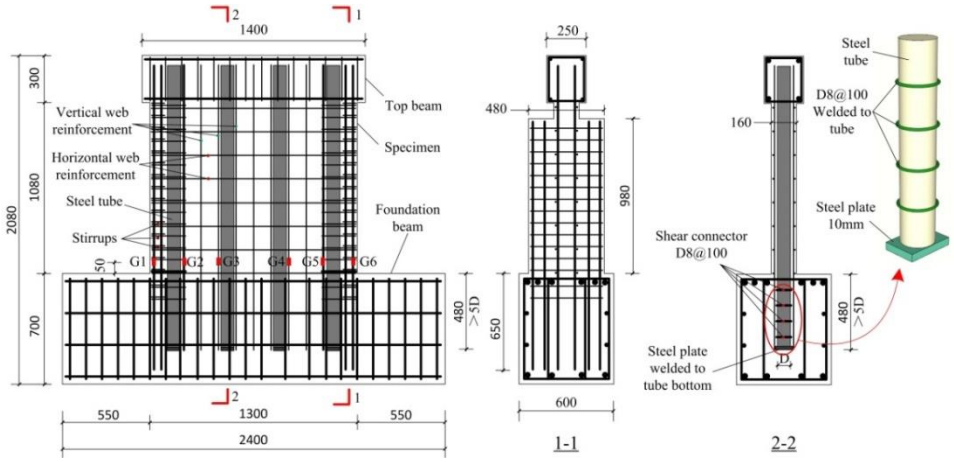

Figure 1. General layout dimensions and reinforcement arrangement of the specimens (Unit: mm).

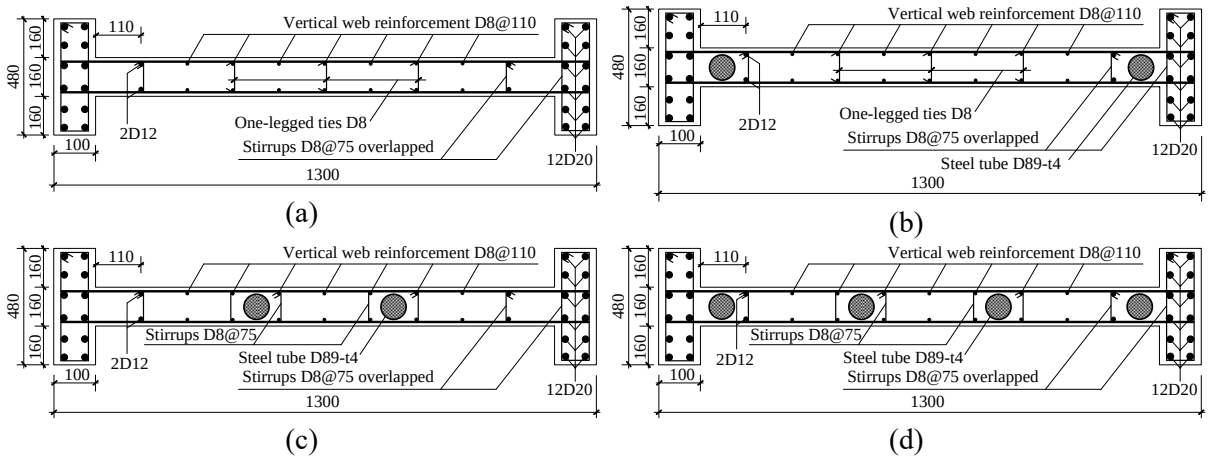

Figure 2. Sectional dimensions and reinforcement details of specimens (Unit: mm): (a) SW1; (b)SW2/SW3; (c) SW4/SW5; (d) SW6.

2.2. Material properties

The measured yield and ultimate strengths of steel rebars are summarized in Table 1. The steel tubes were made up of Grade Q345 steel. The material properties of steel tubes, used in the tests, are also reported in Table 1. The concrete that filled in the steel tube had the same strength grade with that outside the tube. The average cube strength (f_{cu}) at the time of tests is 66.7 MPa.

Table 1. Material properties for steel. (Unit: MPa).

	Rebar D8	Rebar D12	Rebar D20	Steel tube
Yield strength f_y	410	483	443	348
Ultimate strength f_u	587	659	600	416

3. Experimental observations and test results

3.1. Damage and failure mode

Figure 3 shows eventual failure of the four specimens. According to the test of four specimens, the failure model of the high strength concrete squat shear walls with distributed steel tubes was analysed.

SW1 was a RC shear wall. The first crack occurred at the upper left corner of the specimen during the controlled rotation 1/1000, and then extended to the lower right corner. When reaching the peak load (the controlled rotation was 1/100), SW1 failed with the main diagonal crack coalesced which inclined at an angle around 45° to the horizontal direction. Simultaneously, the horizontal reinforcement in the central of the wall fractured, and the longitudinal reinforcement at the lower right corner buckling. The concrete around the main diagonal crack spalling severely and the concrete at the lower right corner crushed. The eventual failure was the brittle shear failure mode along the main diagonal crack, as shown in Figure 3(a).

SW2 was the squat wall with steel tubes arranged at both sides. The first crack occurred at the upper right corner of the specimen during the controlled rotation 1/2000. When the controlled rotation was 1/250, large numbers of 45° skew cracks occurred at the middle of the web of the wall, some of which developed as the main diagonal cracks at further stage. When the controlled rotation was 1/100, two main diagonal cracks appeared apparently with the concrete at the intersection crushed severely. When the controlled rotation was 1/75, the concrete at the intersection of two main diagonal cracks was almost completely peeled off, and the vertical web reinforcement buckling, as shown in Figure 3(b). Compared with SW1, the damage of SW2 was more homogeneous before the peak load of SW1, and the damage was mainly concentrated in the middle part of the specimen, as shown in Figure 4.

SW3 was the squat wall with steel tubes arranged at the middle section. The first crack occurred at the controlled rotation 1/2000. In the initial stage of 1/500 cycle, several skew cracks appeared on the left side of the wall. However, the propagation of the cracks was suppressed because of the existence of steel tubes, and there were some cross bond cracks at the position of steel tubes at the meantime. When the controlled rotation was 1/75, large area of concrete spalling between the two steel tubes occurred, and the spalling area of concrete made up around 1/3 of the total area of the wall. When the controlled rotation was 1/50, the root of the left flange of the wall damaged severely, along with significantly load-carrying capacity deterioration, as shown in Figure 3(c).

SW4 was a squat wall with steel tubes evenly distributed in the cross-section of the specimen. The first crack occurred at the upper right corner of the specimen during the controlled rotation 1/1000. When the controlled rotation was 1/500, the development of inclined cracks was obviously suppressed by the steel tubes. However, the bond crack zone along the height direction of the steel tube formed apparently. During the 1/50 cycles, concrete along the height direction of steel tubes spalling severely, and four steel tubes exposed. When the controlled rotation was 1/30, the concrete cover in the web of the wall was almost completely lost, along with slight damage of flanges, as shown in Figure 3(d). There was no obvious shear failure in the specimen. SW4 exhibited excellent deformation capacity and stability and worked in a way similar to the rocking wall [8] at the later stage.

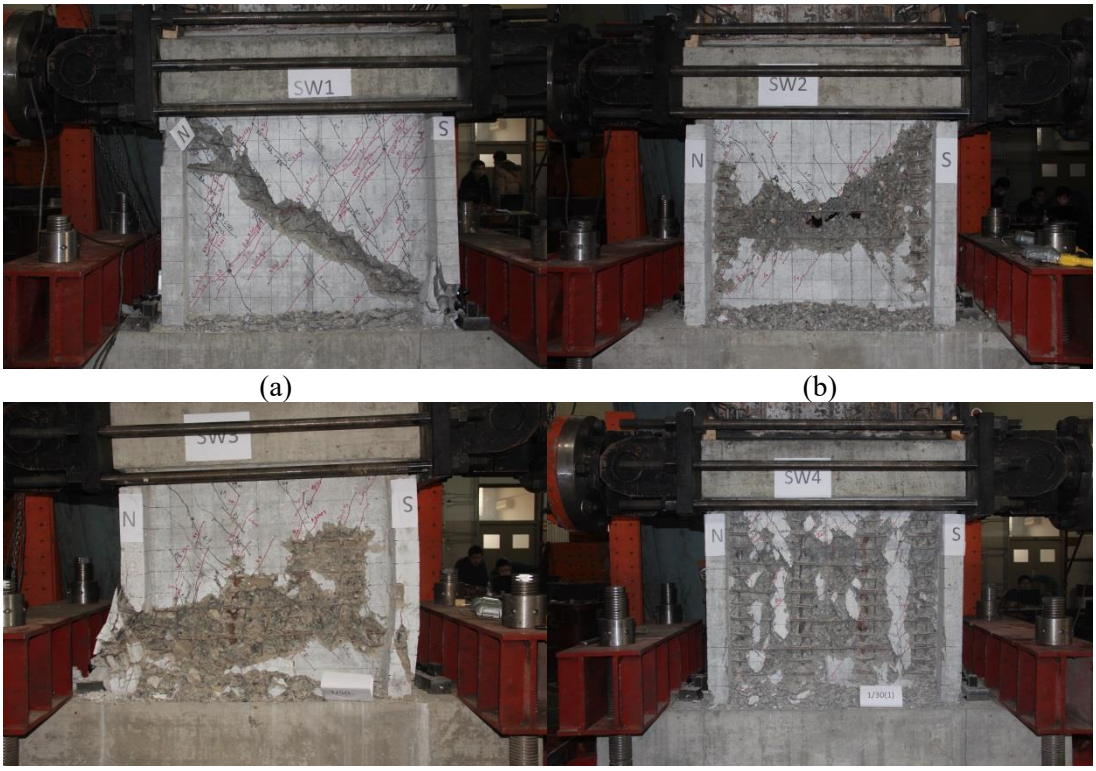

Figure 3. The failure modes of the specimens: (a) SW1; (b)SW2; (c) SW3; (d) SW4.

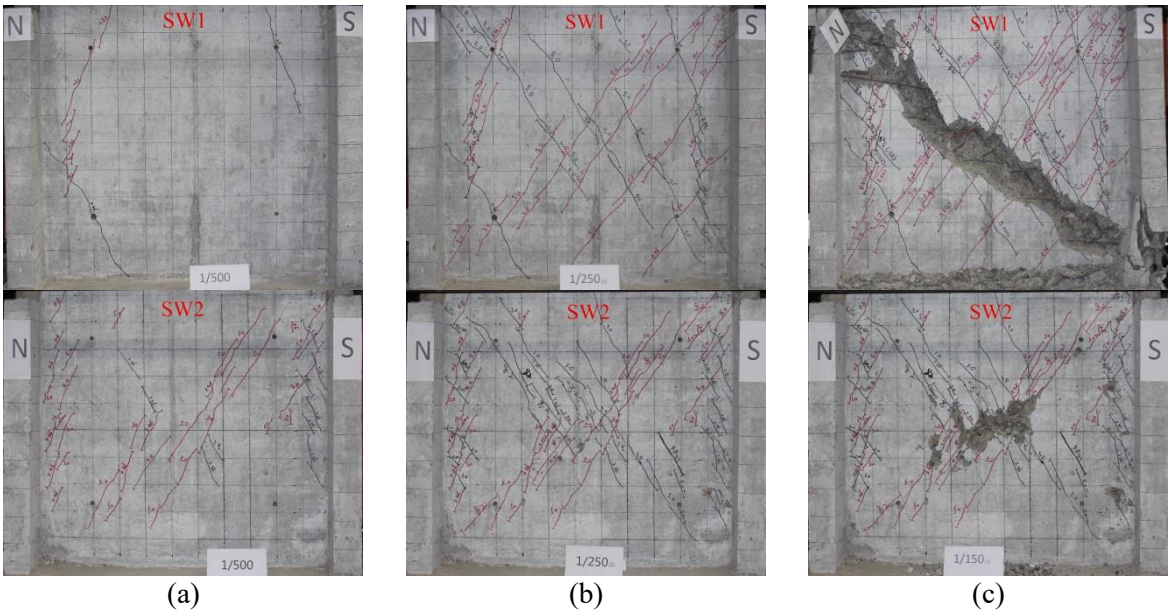

Figure 4. Comparison of damage evolution between SW1 and SW2: (a) 1/500; (b) 1/250; (c) 1/150.

As seen from the above description, steel tubes could not delay the time that the first crack occurred. After inserted steel tubes, the development of inclined cracks was suppressed obviously, thus avoiding the brittle failure. However, the vertical bond slip cracks would be presented in the connections between steel tubes and the concrete after inserted steel tubes. By comparing the failure mode of SW2 with that of SW3 could be found, steel tubes which inserted into the both sides of the wall could play a role in protecting the flanges, so that the specimen was more stable. The failure mode of the specimen

was no longer a shear failure after steel tubes were evenly inserted into the wall section. SW4 combined the advantages of SW2 and SW3 effectively, and showed a good deformation capacity and stability.

3.2. Force-displacement relationship

The recorded curves of lateral force (P) versus lateral displacement (Δ) for all specimens are shown in Figure 5. It was found that the lateral force versus lateral displacement response of SW1 cycled almost linearly. The specimen behaved approximately elastically with little residual displacement occurred. The energy dissipation and ductility of SW1 were very poor, and the specimen showed the characteristics of brittle failure.

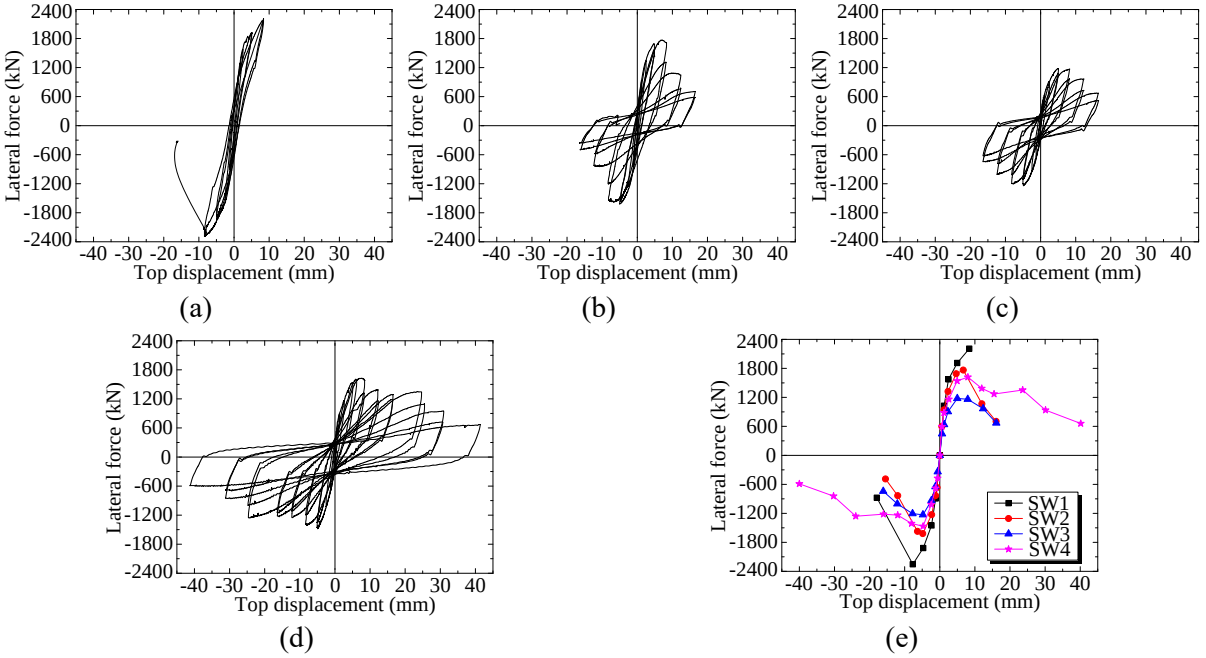

Figure 5. Hysteresis and Skeleton curves: (a) SW1; (b) SW2; (c) SW3; (c) SW4; (e) Skeleton curves**.**

Compared with SW1, SW2 had plumper hysteresis curve, better ductility and plastic deformation capacity. However, load-carrying capacity of SW2 was lower than that of SW3. The damage evolution of SW4 was more homogeneous than that of SW1 due to the insertion of steel tubes. And this caused the damage of SW2 was more severe than that of SW1 at the same controlled rotation before the peak load. This in turn led to the reduction of load-carrying capacity.

The deformation capacity of SW3 was similar to that of SW2. Nevertheless, the load-carrying capacity of SW3 was lower than that of SW2. Firstly, the damage of specimen with steel tubes inserted in the middle section was more severe than that of specimen with steel tubes inserted in the both sides during the same controlled rotation, especially in the flange, and then, the moment capacity of SW2 was higher than that of SW3 due to the steel tubes on both sides. Both contributed to the fact that SW2 had a higher load-carrying capacity.

As shown in Figure 5(d), SW4 exhibited excellent deformation capacity and stability with plump hysteresis curve. Compared with SW2, the load-carrying capacity of SW4 was decreased slightly. It could be noted that the damage at the peak load could be aggravated when the steel tubes inserted into the middle section of squat walls.

Figure 5(e) shows the hysteresis skeleton curves of four specimens. It could be seen that inserted steel tubes, especially in the middle section, would decrease the load-carrying capacity of the squat wall, which could significantly improve the deformation capacity at the same time. The deformation capacity and ductility of the squat wall with steel tubes evenly distributed in the cross-section (SW4) was dramatically improved compared with the other specimens.

4. Analysis of test results and discussions

4.1. Dissipated energy

The dissipated energy in each cycle could be calculated from the lateral load (P) versus lateral displacement (Δ) curve as the area bounded by the hysteretic hoop of that cycle. The single-cycle energy dissipation Es of each specimen is shown in Table 2. The cumulative energy dissipation Ec of each specimen is shown in Figure 6.

The cumulative energy dissipation capacity of specimens, from high to low, was in the following order: SW4, SW2, SW3 and SW1. The single-cycle energy dissipation capacity of SW3 was similar to that of SW1 at the early stage. However, the ultimate cumulative energy dissipation capacity of SW3 was much better than that of SW1 because of the better ultimate deformation. And this phenomenon also occurred between SW4 and SW2. According to observations of the test data, the conclusions are as follows: (1) the effect of steel tubes on the energy dissipation capacity in the squat wall with steel tubes arranged at both sides was slightly better than that of the squat wall with steel tubes arranged at the middle of the section. And the ultimate cumulative energy dissipation capacities were similar because of the similar deformation capacity and single-cycle energy dissipation capacity; (2) the cumulative energy dissipation capacity of the squat wall with steel tubes evenly distributed in the cross-section (SW4) was about three times higher than that of the squat wall with steel tubes arranged at both sides (SW2) or the squat wall with steel tubes arranged at the middle of the section (SW3), in spite of the doubling of the amount of steel used. And the deformation capacity of SW4 was also improved significantly.

Table 2. The single-cycle energy dissipation E_s. (kN m).

Rotation angle/rad	SW1	SW2	SW3	SW4
1/2000	0.296	0.419	0.258	0.326
1/1000	0.713	1.043	0.805	0.946
1/500	2.026	2.957	2.175	2.703
1/250	4.862	7.872	5.922	7.437
1/250	4.683	7.178	5.356	7.985
1/150	8.353	12.915	9.368	12.200
1/150	8.216	10.120	7.719	10.077
1/100		11.396	11.839	15.725
1/100		7.868	8.857	13.512
1/75		9.475	11.309	19.950
1/75		7.469	8.941	18.612
1/50				31.248
1/50				25.280
1/40				26.783
1/40				21.120

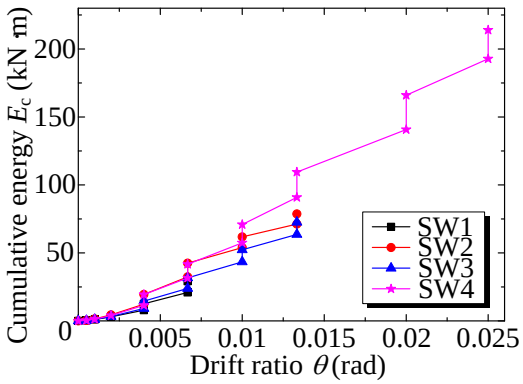

Figure 6. Cumulative energy dissipated of the specimens.

4.2. Rigidity degradation

The stiffness of specimens decreased with the cyclic loading for the reason of cumulative damnification. The stiffness of specimens under cyclic loading can be evaluated by the index-cyclic stiffness, which can be determined as Equation (1):

$$K_l = \sum_{i=1}^{n} P_j^i / \sum_{i=1}^{n} \Delta_j^i \qquad (1)$$

In which, K_l is the cyclic stiffness; P_j^i is the peak load of the *i* th cycle when the deformation is controlled as Δ_j; Δ_j^i is the peak deformation of the *i* th cycle when the deformation is controlled as Δ_j; and n= the number of cycles when the deformation is controlled as Δ_j.

The K_l–Δ curves of specimens are shown in Figure 7. These cyclic stiffness degradation curves are compared, and the analysis can be made as follows:

(1) The initial rigidities of specimens in a lower to higher order were the first for SW3, the second SW1, the third SW4 and the fourth for SW2. The initial rigidity of the squat wall could be improved by inserting steel tubes into both sides of the wall, and could be reduced by inserting steel tubes into the middle section of the wall. The initial stiffness of SW4 was higher than that of SW1, which indicated that the enhancing effect of steel tubes arranged at both sides to the initial stiffness of squat walls was higher than that of steel tubes arranged at the middle section.

(2) Due to the interaction between steel tubes and the concrete, the positive initial stiffness of specimens was larger than the negative initial stiffness. After several hysteresis hoops, the positive stiffness was almost the same as the negative stiffness due to the concrete spalling. In SW4, this characteristic was especially obvious.

(3) In the case of large deformation, the stiffness degradation of SW4 was flat without sundden drop in the stiffness. This kind of wall exhibited excellent deformation capacity and collapse resistant capability.

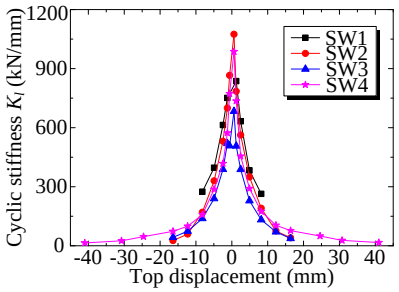

Figure 7. Comparison of K_l–Δ curves of specimens.

4.3. Strain distribution of the section

In order to study the strain distribution of the section of specimens in the process of loading, 6 strain gauges (G1~G6) were arranged at the bottom section of each squat wall, and the distance from the strain gauges to the foundation beam was 50mm, as shown in Figure 1. The strain distributions of states of axial force exerted, cracking, yield, and peak load were shown in Figure 8. The ordinate axis represents the strain measured by strain gauges, and the abscissa axis represents the distance from the strain gauge to the left edge of the wall. Because of the problem of the strain gauge data acquisition, the strain distribution of SW4 was not presented in this paper. Based on the illustrations, the following conclusions could be made: (1) After the axial force was exerted, the strain distributions of SW1 and SW2 were basically in accordance with the plane section assumption. However, due to the existence of steel tubes in the middle section of SW3, the strain of the middle section was smaller than that of the two ends; (2) Before the cracking, the strain distributions of specimens basically obeyed the plane section assumption. However, after squat walls cracking, the strain distributions of specimens was no longer consistent with the plane section assumption.

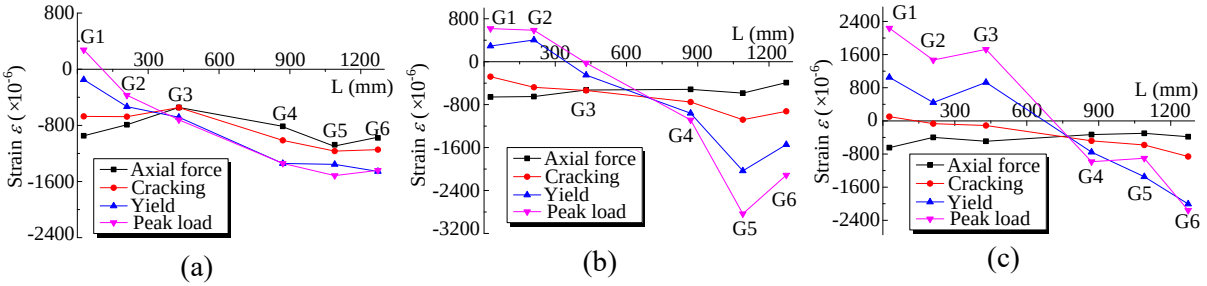

Figure 8. Strain distributions along the bottom sections of the specimens: (a) SW1; (b) SW2; (c) SW3.

5. Conclusions

Three squat walls with steel tubes and one RC squat wall were tested and analysed. The main conclusions can be summarized as follows:

(1) The ordinary high strength concrete squat wall showed a poor ductility and energy dissipation, with obvious brittle shear failure.

(2) The deformation capacity of the high strength concrete squat wall was improved dramatically after the insertion of steel tubes. After inserted steel tubes, the development of inclined cracks was suppressed obviously, and then, the damage evolution of squat walls was more homogeneous at each stage. The deformation capacity and energy dissipation capacity of the squat wall with steel tubes evenly distributed in the section (SW4) were much better than that of any of the first three squat walls. The cumulative energy dissipation capacity of SW4 was about three times higher than that of SW2 or SW3, although the amount of steel tubes doubled.

(3) The initial rigidity of the squat wall could be improved by inserting steel tubes into both sides of the squat wall, and could be reduced by inserting steel tubes into the middle section of the squat wall. And the enhancing effect of steel tubes arranged at both sides to the initial stiffness of squat walls was larger than the weakening effect of steel tubes arranged at the middle section to the initial stiffness of squat walls.

(4) The strain distribution of bottom section of the squat wall was no longer consistent with the plane section assumption after the squat wall cracking. Thus, the plane section assumption was no longer suitable for the calculation of the peak load of the squat wall.

6. References

[1] Parulekar YM, Reddy GR, Vaze KK, Pegon P, and Wenzel H 2014 Simulation of reinforced concrete short shear wall subjected to cyclic loading. *Nuclear Engineering and Design* **270(5)**: 344-350

[2] Abdlebasset YM, Sayed-Ahmed EY, Mourad SA 2016 Seismic analysis of high-rise buildings with transfer slabs: state-of-the-art-review. *Electronic Journal of Structural Engineering* **16(1)**: 38-51.

[3] Su RKL and Cheng MH 2009 Earthquake‐induced shear concentration in shear walls above transfer structures. *The Structural Design of Tall and Special Buildings* **18(6)**: 657-671

[4] Elawady AK, Okail HO, Abdelrahman AA and Sayed-Ahmed EY 2014 Seismic Behaviour of High-Rise Buildings with Transfer Floors. *Electronic Journal of Structural Engineering* **14(2)**: 57-70.

[5] Chen L, Mahmoud H, Tong SM and Zhou Y 2015 Seismic behaviour of double steel plate-HSC composite walls. *Engineering Structures* **102(8)**: 1-12

[6] Hu HS, Nie JG, Fan JS, Tao MX, Wang YH and Li SY 2016 Seismic behaviour of CFST-enhanced steel plate-reinforced concrete shear walls. *Journal of Constructional Steel Research* **119(3)**: 176-189

[7] Qian JR, Jiang Z and Ji XD 2012 Behaviour of steel tube-reinforced concrete composite walls subjected to high axial force and cyclic loading. *Engineering Structures* **36(4)**: 173-184

[8] Nazari M, Sritharan S, Aaleti S 2017 Single precast concrete rocking walls as earthquake force-resisting elements. *Earthquake Engineering & Structural Dynamics* **46(5)**: 753-769.

Acknowledgments
This work presented herein was supported by National Natural Science Foundation of China (Grants No. 51478243). The writers wish to express their sincere gratitude to the sponsor. The writers would also like to thank the anonymous reviewers for their valuable comments and suggestions.